Virial coefficients of rare gases on xenon-plated graphite using image theory

Chung-Yuan Ren[1,2] and Chen-Shiung Hsue[2]
[1]*Department of Electronic Engineering, Kao Yuan Institute of Technology, Kaohsiung, Taiwan 821, Republic of China*
[2]*Institute of Physics, National Tsing Hua University Hsinchu, Taiwan 300, Republic of China*
(Received 31 October 2002; published 19 March 2003)

The first two virial coefficients and their temperature derivatives for Ne and for Ar atoms adsorbed on xenon-plated graphite are reexamined with the implementation of the Mahanty's image theory. On the assumption that the substrate is treated as a good conductor, encouraging values of the second virial coefficient β_2 and the average lateral interaction energy ϵ_2 of an isolated pair of adatoms are obtained when the ''ideal surface'' of the substrate is set at 1.9 Å above the xenon layer, a distance which is essentially identical to the van der Waals radius of the xenon atom. Under such a situation, the strength of the adatom-adatom interaction is weakened by a factor of 0.56 and 0.60 for the Ar and the Ne case, respectively, which are in concord with the predictions asserted in earlier work. Discussions on the dependence on the dielectric constant of the substrate are also given. The present results seem to indicate that the Mahanty's theory provides a viable alternative approach for studies of physisorption problems.

DOI: 10.1103/PhysRevB.67.115411 PACS number(s): 68.43.−h, 68.47.−b, 67.40.Kh, 34.50.Dy

I. INTRODUCTION

Measurement of adsorption heats and isotherms for rare gases adsorbed on xenon-plated graphite offers a relatively clean way to study the dynamics of the interatomic potential between the adatoms. Since the dominant factors involved are the long-range van der Waal's dispersion forces, the results are supposed to be much simpler to analyze and a relatively clear-cut conclusion can be achieved. Several thermodynamic properties which characterize the behavior of isolated adatoms and pairs of adatoms for such systems were first analyzed experimentally by Barnes and Steele.[1] In this respect, with use of the Lennard-Jones LJ(6,12) potential, a systematical study of the virial coefficients for argon adatoms based on Ono's formulas[2] was carried out by Wu.[3] The calculated value ϵ_1 which represents the average potential energy of an isolated adatom was in good agreement with the experiment. It was argued that the so-called configurational integral for a single adatom Z_s was susceptible to improvement with a better pairwise interaction potential and a better value of the separation distance between the xenon layer and graphite. On the other hand, the results for the second virial coefficient for a pair of adatoms β_2 and the average lateral interaction energy of an isolated pair of adatoms ϵ_2 far exceeded the experimental data. Good results could only be obtained by artificially lowering the well depth of the argon-argon interatomic potential by an amount of 30% from its gas phase value. Since the experiments were measured at a very low temperature, these quantities were sensitive to the potential involved. Instead of the simple LJ potential, the same systems of argon and neon adatoms were studied[4,5] by employing exp-6 potentials[6] and various other interatomic potentials, which were obtained from accurate beam-scattering data.[7,8] The calculations of Z_s and ϵ_1 were consistent with the experiment. But even with the inclusion of three-body Axilrod-Teller-Muto (ATM) contributions,[9] the above discrepancy of the second-order quantities persisted.

Actually, the second virial coefficient and the lateral energy of the adatom pair are affected not only by the substrate but also by the interatomic potential between the adatoms. However, since the force exerted on the adatoms by the substrate is quite strong near the surface, the effective interatomic potentials should be carefully investigated for physisorption problems. Sinanoğlu and Pitzer[10] first pointed out that the existence of the surface leads to the modification of the pair attraction in free space. Based on the continuum model, McLachlan[11] derived explicitly a perturbation term to demonstrate the presence of the above effect. A simplified picture to visualize this phenomenon is that the second-order weakening of polarization of the adatom-pair arises due to the interaction from their electrical images. It has been proposed by Brown *et al.*[12] that such a situation occurs when hydrogen molecules are brought up to the surface of platinum. Mahanty and March[13] developed a rigorous theory which states that the nonretarded long-range dispersion interaction between adatoms is weakened near substrates. This is basically a more elaborate extension of the McLachlan's work. It has been further developed and refined by der Hertog and Choy.[14] During the past two decades, the investigation of adatom-pair potentials near substrates has attracted intensive interests in both experimental measurements and theoretical calculations. For example, Bruch[15] made a general discussion on physisorption interactions; Rauber *et al.*[16] investigated the screening of the substrate upon various adsorbates within the McLachlan's framework; Mahanty[17] applied the image theory to study the behavior of the adatoms on jellium models; Gibson and Sibener[18,19] measured the resonances of helium atoms from rare gases physisorbed on Ag(111) and evaluated the potential with the three-body ATM interaction; Aziz and Scoles[20] considered two- and three-body forces in the interaction of helium atoms with xenon layers adsorbed on graphite, etc. Physisorption has become an active and productive area of research.

Generally speaking, both the Mahanty's theory and the ATM contribution are based on the dynamics of the correlation among dipoles. The former manifests itself macroscopically in terms of the dielectric constant of the substrate whereas the latter gives a microscopic description of the in-

teratomic interaction. Therefore, the image theory provides another approach to consider the adsorptive induced interactions.

Mainly motivated by the disappointing results with the inclusion of the ATM contribution in the previous work,[4,5] we examine the validity of the Mahanty's image theory in the study of the first two virial coefficients and their temperature derivatives for argon and neon adatoms adsorbed on xenon-plated graphite. Substantially improved values for β_2 and ϵ_2 are obtained. The discussion of their possible physical implications will be presented in Sec. IV. A brief description of the virial expansion for physisorption and the image theory is given in Sec. II. In Sec. III, we outline how these schemes are implemented in the present work. Finally, a conclusion is given in Sec. V.

II. FORMALISM

A. The virial expansion for physisorption

Following Ono,[2] the expressions for the number of adatoms per unit area θ and the pressure of the adatoms p are given by

$$\theta=\sum_{l=1}^{\infty} l\gamma_l\lambda^l, \tag{1}$$

$$p=\frac{1}{\beta}\sum_{l=1}^{\infty} b_l\lambda^l, \tag{2}$$

where λ is the activity, b_l is the bulk lth cluster integral, and γ_l is the surface lth cluster integral, respectively. Here β is the usual notation for $(k_BT)^{-1}$. In sufficiently dilute gas systems, Eq. (2) can be replaced by the expression for an ideal gas

$$\beta p v_0=\lambda, \tag{3}$$

with $v_0=(h^2\beta/2\pi m)^{3/2}$. The virial series up to the second order of Eq. (1) then becomes as

$$\beta p v_0=\frac{1}{\gamma_1}\left(\theta-2\frac{\gamma_2}{\gamma_1^2}\theta^2\right)+O(\theta^3), \tag{4}$$

with

$$\gamma_1=\frac{1}{av_0}\int h(\mathbf{r})d\mathbf{r}, \tag{5}$$

and

$$\gamma_2=\frac{1}{2av_0^2}\int\int d\mathbf{r}_1 d\mathbf{r}_2 h(\mathbf{r}_1)h(\mathbf{r}_2)f(\mathbf{r}_1,\mathbf{r}_2) + \frac{1}{av_0^2}\int\int d\mathbf{r}_1 d\mathbf{r}_2 h(\mathbf{r}_1)f(\mathbf{r}_1,\mathbf{r}_2). \tag{6}$$

Here a represents the total surface area, and $h(\mathbf{r})$ and $f(\mathbf{r}_1,\mathbf{r}_2)$ are given by

$$h(\mathbf{r})=\exp[-\beta V_1(\mathbf{r})]-1, \tag{7}$$

$$f(\mathbf{r}_1,\mathbf{r}_2)=\exp[-\beta V_2(\mathbf{r}_1,\mathbf{r}_2)]-1, \tag{8}$$

where V_1 and V_2 are, respectively, the adatom-surface potential and the pair potential. Equation (4) is the adsorption isotherm and is usually expressed as

$$\beta p=\frac{1}{Z_s}(\theta-\beta_2\theta^2). \tag{9}$$

Here Z_s, the configurational integral for a single adatom, and β_2, the second virial coefficient for a pair of adatoms, are defined as

$$Z_s=v_0\gamma_1, \tag{10}$$

$$\beta_2=\frac{2\gamma_2}{\gamma_1^2}. \tag{11}$$

In addition to the adsorption isotherm, the isosteric heat of adsorption q_{st} is also measured frequently. It is calculated from the thermodynamics relation

$$q_{st}=-(\partial\ln p/\partial\beta)_\theta, \tag{12}$$

which in conjunction with Eq. (4) yields

$$q_{st}=k_BT-(\epsilon_1+\epsilon_2\theta). \tag{13}$$

The classical average potential energy of an isolated adatom ϵ_1 and the average lateral interaction energy of an isolated pair of adatoms ϵ_2 are written down explicitly as follows:

$$\epsilon_1=-\frac{\partial}{\partial\beta}\ln Z_s, \tag{14}$$

$$\epsilon_2=-\frac{\partial}{\partial\beta}\beta_2. \tag{15}$$

B. The image theory

The long-range attractive part of the interatomic potential is essentially the London nonretarded dispersion interaction of the form

$$V(\rho)=-A_{London}/\rho^6. \tag{16}$$

Here ρ is the interatomic distance and A_{London} is the London dispersion force constant.[21] In the theory of Mahanty and March[13] the force constant of an adatom pair, at a distance z from the substrate, is modified with a weakening function F,

$$A'=A_{London}F. \tag{17}$$

In the case when the adatom pair is parallel to the surface, F is written in terms of the dielectric constant ϵ_d of the substrate and the variable $s=2z/\rho$ as

$$F=F(s;\epsilon_d)=1+\frac{\Delta^2}{(1+s^2)^3}-\frac{4\Delta(1+s^2/4)}{3(1+s^2)^{5/2}}, \tag{18}$$

$$\Delta\equiv(\epsilon_d-1)/(\epsilon_d+1). \tag{19}$$

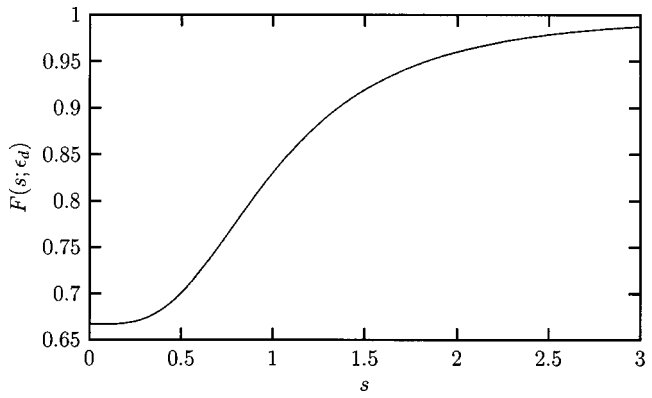

FIG. 1. The behavior of the weakening factor $F(s;\epsilon_d)$ when the substrate is an ideal conductor.

The derivation of Eq. (18) is based on the appropriate Green's function **G** connecting the electric field at **r** to a dipole source $\mu(\omega)$ at $\mathbf{r}'$ with a frequency ω, i.e.,

$$\mathbf{E}(\mathbf{r})=\mathbf{G}(\mathbf{r},\mathbf{r}';\omega)\mu(\omega). \tag{20}$$

Taking the dielectric surface to be the x-y plane with both **r** and $\mathbf{r}'$ outside the dielectric, we have the Green's function in the following form by use of the usual method of images:

$$\mathbf{G}(\mathbf{r},\mathbf{r}';\omega)=\mathbf{G}_{\mathrm{D}}(\mathbf{r},\mathbf{r}')-\Delta\,\mathbf{G}_{\mathrm{I}}(\mathbf{r},\mathbf{r}'), \tag{21}$$

$$\mathbf{G}_{\mathrm{D}}(\mathbf{r},\mathbf{r}')\equiv-\nabla\nabla'\frac{1}{|\mathbf{r}-\mathbf{r}'|}, \tag{22}$$

$$\mathbf{G}_{\mathrm{I}}(\mathbf{r},\mathbf{r}')\equiv-\nabla\nabla'\frac{1}{|\mathbf{r}-\mathbf{r}'_{\mathrm{im}}|}. \tag{23}$$

The $\mathbf{G}_{\mathrm{D}}(\mathbf{r},\mathbf{r}')$ is due to the free-space dipole source at $\mathbf{r}'$ and $\mathbf{G}_{\mathrm{I}}(\mathbf{r},\mathbf{r}')$ is the indirect part, arising through the screening of the dielectric medium. Here $\mathbf{r}'_{\mathrm{im}}$ is the image of the point $\mathbf{r}'$. By keeping only the leading order in the polarizabilities, the effective dispersion interaction energy for the adatom pair can be expressed as[13]

$$E_{12}=-\frac{\hbar}{4\pi}\int_{-\infty}^{\infty}d\xi\alpha_1(i\xi)\alpha_2(i\xi)\mathrm{Tr}[\mathbf{G}(\mathbf{r}_2,\mathbf{r}_1)\mathbf{G}(\mathbf{r}_1,\mathbf{r}_2)]. \tag{24}$$

When the pair is parallel to the surface, the trace of the Green's functions is evaluated straightforwardly as

$$\mathrm{Tr}[\mathbf{G}(\mathbf{r}_2,\mathbf{r}_1)\mathbf{G}(\mathbf{r}_1,\mathbf{r}_2)]=\frac{6}{\rho^6}+\frac{6\Delta^2}{(\rho^2+4z^2)^3}-\frac{8\Delta(\rho^2+z^2)}{\rho^3(\rho^2+4z^2)^{5/2}}. \tag{25}$$

Inserting Eq. (25) into Eq. (24), we obtain the weakening function $F(s;\epsilon_d)$ of Eq. (18) by identifying A_{London} with $(3\hbar/2\pi)\int_{-\infty}^{\infty}\alpha_1(i\xi)\alpha_2(i\xi)d\xi$.[21] The function $F(s;\epsilon_d)$ for the case when the substrate is a perfect conductor is explicitly shown in Fig. 1. It is seen that in such a case the weakening factor varies monotonically from 2/3 to 1.

III. APPLICATION TO ADATOMS ON XENON-PLATED GRAPHITE

Since the Mahanty's theory is based on the dynamics of dipole-dipole correlation, only the dispersion part r^{-6} of the interatomic potential should be modified. Therefore, even though there are more sophisticated potentials, e.g., the Morse-Spline-van der Waals form or the Hartree-Fock Dispersion form,[7,8,22] which gives an accurate description of the pairwise interaction, these refinements are not applicable to this theory due to their mixture of other dispersion types. In addition, utilization of the same potential models employed in the previous work[3–5] will illustrate the significance of the image effect more clearly. Thus the simple LJ(6,12) and exp-6 models are still used here for comparisons.

A. The standard Lennard-Jones potential

This is the simplest model for the interatomic potential, which reads

$$V_2=4\epsilon_{Y-Y}\left[\left(\frac{\sigma_{Y-Y}}{r}\right)^{12}-\left(\frac{\sigma_{Y-Y}}{r}\right)^{6}\right]. \tag{26}$$

The subscript Y stands for Ne or Ar.

B. The exp-6 model suggested by Hogervorst

The interatomic potential in this model[6] is written as

$$V_2=\frac{\epsilon}{1-6/\alpha}\left\{\frac{6}{\alpha}\exp\left[\alpha\left(1-\frac{r}{r_m}\right)\right]-\left(\frac{r_m}{r}\right)^6\right\}, \tag{27}$$

with r_m as the interatomic distance for the minimum potential energy ϵ and α as a factor determining the hardness of the repulsive part of the potential.

With the presence of xenon monolayer located at a distance 3.66 Å on top of the graphite,[23] the separation between the adatoms and the carbon atoms of graphite is relatively large. As a result, the repulsive effect of the Y-carbon interaction can be omitted completely and only the attractive part needs to be taken into account. Furthermore, the discrete distribution of carbon atoms in a single layer may be replaced by an equivalent uniform distribution. The adatom-graphite interaction potential is then given by[23]

$$V_{Y-C}=-\epsilon_{Y-C}\sum_{l=0}^{\infty}(l+z'/d)^{-4}. \tag{28}$$

Here $d=3.35$ Å is the interplanar spacing of the graphite, and z' is the distance between the adatom and the first carbon layer. Consequently, the adatom-surface potential for the LJ type is expressed as

$$V_1(\mathbf{r})=4\epsilon_{Y-\mathrm{Xe}}\sum_i\left[\left(\frac{\sigma_{Y-\mathrm{Xe}}}{R_i}\right)^{12}-\left(\frac{\sigma_{Y-\mathrm{Xe}}}{R_i}\right)^{6}\right]-\epsilon_{Y-\mathrm{C}}\sum_{l=0}^{\infty}(l+z'/d)^{-4}, \tag{29}$$

TABLE I. The relevant constants in LJ(6,12) potentials.

Y	$\epsilon_{\text{Y-Xe}}$ (K)	$\sigma_{\text{Y-Xe}}$ (Å)	$\epsilon_{\text{Y-Y}}$ (K)	$\sigma_{\text{Y-}Y}$ (Å)	$\epsilon_{\text{Y-C}}$ (K)
Ar[a]	166	3.74	124	3.40	1782
Ne[b]	91.13	3.39	36.38	2.82	531.5

[a]Reference 3.
[b]Reference 5.

where

$$R_i = |\mathbf{r} - \mathbf{R}_i'|, \tag{30}$$

and $\mathbf{R}_i'$ is the location of the ith xenon atom. The corresponding $V_1(\mathbf{r})$ for the exp-6 type can be similarly obtained by replacing the first term on the right-hand side of Eq. (29) by Eq. (27). The relevant potential parameters are listed in Tables I and II.

The experimental data of Ref. 1 were obtained by assuming that the xenon layer was squared packed, with an area of 18.6 A^2 for a unit cell. However, the xenon atoms on graphite prefer a hexagonal structure instead. In previous works[3–5] the simple $\sqrt{3}\times\sqrt{3}\mathbf{R}$ 30° model, with a lattice constant of 4.26 Å, was used for the calculation. Furthermore, an immense amount of more sophisticated experiments[20,25–28] have shown that the periodicity imposed by the graphite potential is different from that favored by the xenon atoms and the resultant hexagonal structure is distorted in the misfit-dislocation domain. To reduce the degree of complexity, we assume that the xenon layer still has a hexagonal array with a larger averaged lattice constant of 4.30 Å (Ref. 20) to take into account of both the incommensuration with respect to the substrate and the contribution of the distortion. Besides, the fractional coverage $\tilde{\theta}$ in Ref. 1 was defined as the number of adatoms per unit cell rather than per unit area, it is therefore necessary to make a suitable modification on the definitions of Z_s, β_2, and ϵ_2 for a better comparison with the experiment. From Eqs. (5), (9), (10), and the relation

$$\tilde{\theta} = N_s/a/(18.6\ \text{Å}^2) = (18.6\ \text{Å}^2)\,\theta, \tag{31}$$

where N_s is the total number of the adatoms, we modify Z_s as

$$Z_s = \frac{18.6\ \text{Å}^2}{u}\int_\Omega h(\mathbf{r})\,d\mathbf{r}. \tag{32}$$

Here u is the area of a unit cell and the integration is taken over the whole volume Ω above the unit cell. A similar deri-

TABLE II. The relevant constants in exp-6 potentials.

	ϵ(K)	α	r_m(Å)
Ar-Xe [a]	188	15.0	4.07
Ar-Ar [b]	123	14.0	3.87
Ne-Xe [a]	69	15.0	3.91
Ne-Ne [b]	38	14.5	3.15

[a]Reference 24.
[b]Reference 6.

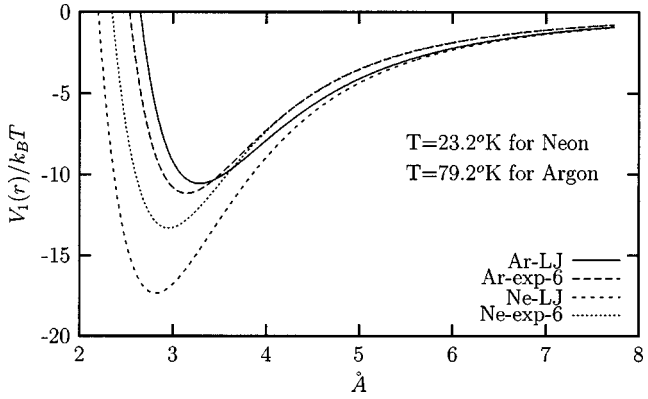

FIG. 2. Profiles of the surface potentials for both argon and neon adatoms at the center of the triangle lattice as a function of the distance between the adatom and the xenon plane. The distances for the minimum of the surface potential are 3.29 Å, 3.15 Å, 2.82 Å, and 2.95 Å for Ar-LJ, Ar-exp-6, Ne-LJ, and Ne-exp-6 cases, respectively.

vation shows that both quantities β_2 and ϵ_2 should be divided by the factor $(18.6\ \text{Å}^2)/u$.

For an efficient evaluation of γ_1 and γ_2, it is useful to take into account the behavior of $h(\mathbf{r})$ to arrive at accurate results. Figure 2 displays the values of $V_1(r)/(k_BT)$ at the center of the triangle as a function of the distance between the adatom and the xenon plane. It is clear that the weighting factor $h(\mathbf{r})$ is extremely large, about 10 000, only around the vicinity of the potential minimum. Thus, it is important to maintain the greatest accuracy for the integration near the maximum of $h(\mathbf{r})$, which accounts for most of the contribution to the integral. In addition, the second term on the right-hand side of Eq. (6), which contains only one factor of $h(\mathbf{r})$, can be safely dropped out in comparison with the first dominant term.

In actual calculations, due to the strong repulsive interaction when the adatoms are near the substrate and the rapid decaying for the magnitude of the effective potential when the adatoms are far away from the surface, it is found that only a very narrow range along the z axis yields significant contribution to the integration. In the present work, the range is set to be [0.6,1.2] and [0.5,0.9] (in units of 4.30 Å) for the Ar and the Ne case, respectively. Different orders of Gauss-Legendre quadratures[29] are then employed for the integration. The contributions beyond these intervals are negligible. The integrations over the area of the unit cell are carried out with the aid of a seven-point formula.[30] The rate of convergence for the result is extremely fast if the unit cell is sectioned into aggregates of equilateral triangles appropriately in accordance with the behavior of $h(\mathbf{r})$ or $f(\mathbf{r},\mathbf{r}')$. From numerical comparisons it is found that the evaluation with 49 integrating points in the half unit cell is enough to ensure an accuracy up to fourth digits. This efficient algorithm is essential for the evaluation of γ_2, which contains a six-dimensional integration. The sum over xenon atoms in Eq. (29) is carried out over the nearest 75 atoms, with a uniform-density approximation taking into account the contributions from those further away.[5] As to the adatom-graphite interaction, we first calculate the first six terms of the series and the

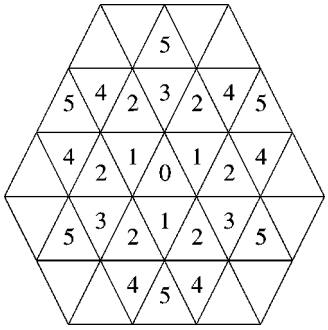

FIG. 3. Rings of equivalent half-lattice zones.

remaining contributions can then be obtained by the asymptotic trigamma-function expansions.[5] For the treatment of the $f(\mathbf{r}_1,\mathbf{r}_2)$ term in the γ_2, only the first four nearest rings, see Fig. 3, are considered. By a ring we mean the equivalent half lattices with equal distances from the origin. The contributions from the fifth ring and further far away can be omitted.

With the implementation of the Mahanty's image theory, the strength of the pair attraction is modified with the weakening factor $F(s;\epsilon_d)$ through Eqs. (17) and (18). Figure 1 shows that the $F(s;\epsilon_d)$ stays close to the minimum value 2/3 when s is smaller than 0.5; and quickly increases to the value near unity as s is varied from 0.5 to 2.0. This indicates that for a fixed interatomic separation ρ the dependence of $F(s;\epsilon_d)$ on the distance z, which represents the distance of the adatom pair from the substrate surface, is rather subtle, especially near the vicinity of the surface. For the present physisorption systems, the typical value of ρ is of the order of the lattice constant ($\sim$4.30 Å), as illustrated in Fig. 3. As a result, the potential between the adatoms is significantly weakened when the adatom pair is at a distance of $\sim$2 Å from the surface. On the contrary, the image effect becomes small as the pair is located at $\sim$4 Å away. However, this range is not large on the scale of the thickness of the real ''surface'' itself. This means that an unambiguous position of the surface required by the image theory is not easily identified. To remedy the ambiguity of the interface, the concept of an ideal surface, referred to as a *reference* plane in Fig. 4, is proposed. The virial coefficients and their temperature derivatives are then investigated with a series of different positions for the reference planes. Moreover, to simplify the calculation, the substrate, which is composed of the xenon monolayer and graphite, is assumed as a perfect metal bulk.

IV. RESULTS AND DISCUSSIONS

A. Ar adatoms

The experiment for the Ar physisorption was carried out at a temperature of 79.2 K.[1] The calculated values of Z_s and ϵ_1 show that these single-adatom properties are independent of the assumed position of the reference plane. This is expected since, from Eqs. (7) and (32), these two quantities are related to the adatom-surface potential V_1 only, which should not depend upon the reference-plane position. The Z_s from the LJ model is calculated as 10.2 cm^3/site and a larger result of 12.9 cm^3/site is obtained from the exp-6 model. The measured data is 5.39 ± 0.16 cm^3/site. As was discussed before,[4,5] the Z_s is sensitive to the behavior of the potential model used. It is seen, from Fig. 2, that the exp-6 potential has a deeper well and therefore results in a worse value of Z_s. The error in the Z_s can be removed by use of accurate interatomic potential obtained from beam-scattering data.[4,8] Actual numerical computations also reveal that the final results of Z_s are sensitive to the adopted lattice constant of the xenon monolayer. For instance, the incorrect lattice constant of 4.26 Å leads to a worse result of 11.1 cm^3/site in the LJ model. Thus correct geometric structures of the xenon monolayer are essential for accurate values of Z_s. In contrary to Z_s, the ϵ_1 is less sensitive to the above factors, due to the logarithm dependence in Eq. (14). The calculated value of ϵ_1 is found to be -708 K and -745 K for the LJ and exp-6 models, respectively. They are close to the experimental data of -700 ± 21 K.

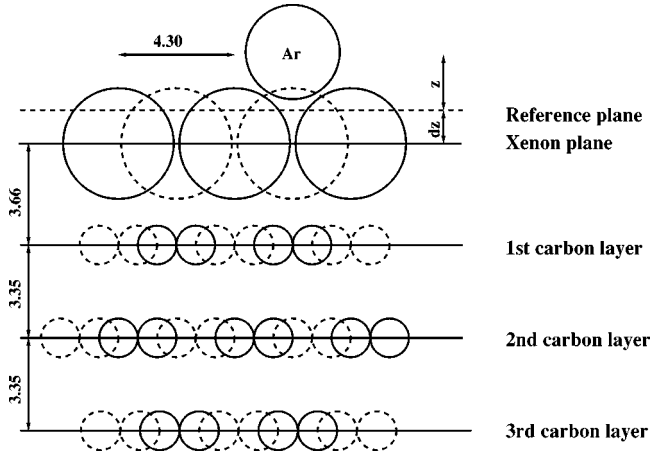

FIG. 4. Geometry of the adatoms absorbed on the xenon-plated graphite. The reference plane serves as the ''ideal surface'' of the substrate with the implementation of the image theory. Here, the lengths are given in units of angstrom.

The results of the second-order coefficient β_2 and its temperature derivative ϵ_2 for various positions of reference planes are summarized in Table III. Several interesting features are observed from this table. First of all, combined with the image effect, there is a remarkable variation of the magnitudes for β_2 and ϵ_2 as the reference-plane position is varied. In particular, all these values are lower than the ''unmodified'' ones, which are obtained without use of the image theory. To make a comparison, consider the case when the reference plane coincides with the xenon layer. The corresponding values of β_2 and ϵ_2 in the LJ scheme are reduced from 4.87 to 3.88 and -863 K to -685 K, respectively. Hence, the inclusion of the image correction yields much better results.

Second, the results with the image contributions can be significantly improved by moving the reference plane further up above the xenon layer, whereas they converge to the unmodified results when the reference plane is moved in the opposite direction. This is a direct consequence of the asymptotic behavior of the weakening function $F(s;\epsilon_d)$. When the reference plane is set below the xenon layer, the

TABLE III. The second virial coefficient β_2 and the average lateral interaction energy ϵ_2 of an isolated argon pair for various reference planes under LJ and exp-6 models. "−" and "+" in column 1 mean that the reference plane is below and above the xenon layer, respectively. The lattice constant of the xenon layer is 4.30 Å.

Distance (Å)	β_2		ϵ_2 (K)	
	LJ	exp-6	LJ	exp-6
−2.00	4.55	4.56	−807	−819
−1.90	4.54	4.54	−804	−816
−1.80	4.52	4.52	−801	−812
−1.70	4.50	4.51	−797	−809
−1.60	4.48	4.48	−794	−805
−1.50	4.46	4.46	−790	−801
−1.40	4.44	4.44	−786	−797
−1.30	4.41	4.41	−781	−792
−1.20	4.39	4.39	−777	−788
−1.10	4.36	4.36	−771	−782
−1.00	4.33	4.33	−766	−777
−0.90	4.30	4.29	−760	−771
−0.80	4.26	4.26	−754	−764
−0.70	4.23	4.22	−747	−757
−0.60	4.19	4.18	−740	−750
−0.50	4.14	4.14	−733	−742
−0.40	4.10	4.09	−724	−733
−0.30	4.05	4.04	−716	−724
−0.20	4.00	3.98	−706	−715
−0.10	3.94	3.92	−696	−704
0.00	3.88	3.86	−685	−693
+0.10	3.82	3.79	−674	−681
+0.20	3.75	3.72	−661	−668
+0.30	3.67	3.64	−648	−655
+0.40	3.59	3.56	−634	−640
+0.50	3.51	3.47	−619	−625
+0.60	3.41	3.38	−604	−609
+0.70	3.32	3.28	−587	−592
+0.80	3.21	3.18	−569	−574
+0.90	3.11	3.06	−551	−556
+1.00	2.99	2.95	−532	−536
+1.10	2.87	2.83	−512	−517
+1.20	2.74	2.70	−491	−496
+1.30	2.61	2.57	−470	−476
+1.40	2.47	2.44	−449	−455
+1.50	2.33	2.30	−427	−435
+1.60	2.19	2.16	−406	−414
+1.70	2.05	2.03	−385	−395
+1.80	1.90	1.89	−364	−376
+1.90	1.76	1.76	−344	−359
+2.00	1.62	1.64	−325	−343
+2.10	1.48	1.52	−308	−328
Unmodified	4.87	4.88	−863	−875
Wu[a]	4.36±0.34		−861±130	
ATM[b]	5.00±0.64		−847±127	
Expt.[c]	1.77±0.35		−420±105	

[a]References 3.
[b]Reference 4.
[c]Reference 1.

separation between the reference plane and the adatom pair is also increased and the value of $F(s;\epsilon_d)$ is close to 1, which means that the image effect is marginally small. On the other hand, this effect will be enhanced as the reference plane is moved above the xenon layer. In particular, by setting the reference planes at positions of 1.7–2.1 Å above the xenon plane, the values for both β_2 and ϵ_2 are brought to be in excellent agreement with the experiment. These values (1.7–2.1 Å) are quantitatively similar to the van der Waals radii of xenon atoms. Intuitively, they locate the reference plane at the edge of the substrate, with the consideration of the rigidity of the electron cloud of the xenon atom. Furthermore, these results are consistent with the work of Zaremba and Kohn,[31] where the polarization potential between a neutral atom and a crystalline solid surface was considered and it was concluded that the reference-plane position is exactly half the distance of the interplanar of the solid if the interaction is taken to be a van der Waals type varying as r^{-6}. Therefore, within the experimental uncertainty, it is tempting to set a definitive position of the reference plane at 1.9 Å ($1.9 \simeq 3.66/2$) above the xenon layer.

Under such a condition, we probe the change of the well depth of the Ar-Ar potential due to the image effect. The most stable position of the pair, within the LJ model, is calculated to be at 3.29 Å above the xenon plane. The profile of the interatomic potential influenced by image effect is presented in Fig. 5(a). The well depth is lowered from −124.00 K (of the free gas phase) to −69.58 K. This means that the reduction factor $f_{\text{Ar-Ar}}$ is 0.56, which is consistent with the prediction of 0.6 asserted in the earlier work.[3,4] For comparisons, we also display in Fig. 5(a) the pair potential when the reference plane is located at a position 2.0 Å below the xenon monolayer. The well depth differs very slightly by a minor amount of 4.04 K, with the lowering rate less than 3%. Similar conclusions are obtained within the framework of the exp-6 model.

Finally, the earlier results[4] of including the Ar-Ar-Xe three-body effect, labeled "ATM" in Table III, are also shown here. The value for β_2 and ϵ_2, evaluated with the accurate beam-scattering interatomic potential,[7] was 5.00 and −847 K, respectively. These are rather disappointing, which could reflect the inadequacy of the three-body contribution in the present situation.

B. Ne adatoms

The experiment for the Ne physisorption was carried out at a low temperature of 23.2 K.[1] In this case, the virial coefficient Z_s is extremely sensitive to the interatomic potential model. The calculated value is 2376×10^{-20} cm^3/site for the LJ model and 67×10^{-20} cm^3/site for the exp-6 potential. The exp-6 model, as displayed in Fig. 2, has a more shallow minimum and a more localized profile, and yields better results. The discrepancy between this value and the experimental number (1.69×10^{-20} cm^3/site) reflects the sensitive exponential dependence on the energy/temperature scale at such a low temperature and the demand of an accurate interatomic potential. More details were discussed in Ref. 5. The

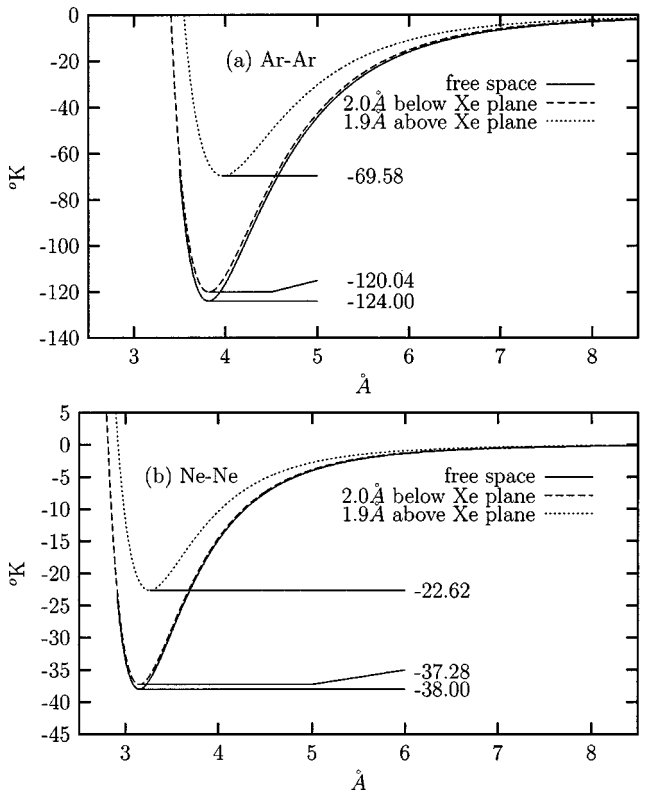

FIG. 5. Interatomic potentials with the image effect for (a) Ar-Ar pairs in LJ models and (b) Ne-Ne pairs in exp-6 models when the reference plane is set 2.0 Å below and 1.9 Å above the xenon plane, along with that in free space. The most stable position of the argon pair and the neon pair is 3.29 Å and 2.95 Å above the xenon plane, respectively.

calculation for the average potential energy of the isolated neon ϵ_1 is -360 K using the LJ model. The corresponding result in the exp-6 model is -266 K. This is close to the experimental value of -240 ± 7.2 K.

Table IV lists the calculated two-particle quantities of β_2 and ϵ_2 for various reference planes. The results from the LJ model are relatively smaller than those from the exp-6 potential. This is primarily due to the fact that β_2 is proportional to the inverse square of Z_s through Eq. (11). It is also shown from this table that these second-order quantities are in best agreement with the experimental values when the optimized position of the reference plane is placed at 1.9 Å above the xenon layer, in consistent with the situation of argon physisorption.

In a similar analysis for the argon adsorption, we study the change of the well depth of the neon-neon interaction with the same optimized position of the reference plane. The resultant interatomic potential is displayed in Fig. 5(b). The most stable position of the neon pair is found to be at 2.95 Å above the xenon plane within the exp-6 model. The well depth in such a situation is weakened from -38.00 K (of the free gas phase) to -22.62 K, with an effective reduction factor $f_{\text{Ne-Ne}}$ of 0.60, which lies in the range between 0.60 and 0.65 suggested before.[5] On the other hand, the well depth of the pair potential is essentially unaltered if the reference plane is placed at 2.0 Å below the xenon layer.

TABLE IV. The second virial coefficient β_2 and the average lateral interaction energy ϵ_2 of an isolated neon pair for various reference planes under LJ and exp-6 models. "$-$" and "$+$" in Column 1 mean that the reference plane is below and above the xenon layer, respectively. The lattice constant of the xenon layer is 4.30 Å.

Distance (Å)	β_2		ϵ_2 (K)	
	LJ	exp-6	LJ	exp-6
-2.00	2.81	3.08	-101	-127
-1.90	2.80	3.07	-100	-127
-1.80	2.79	3.07	-100	-126
-1.70	2.78	3.06	-100	-126
-1.60	2.77	3.05	-99	-126
-1.50	2.75	3.04	-99	-125
-1.40	2.74	3.03	-98	-125
-1.30	2.73	3.02	-98	-124
-1.20	2.71	3.00	-97	-124
-1.10	2.69	2.99	-96	-123
-1.00	2.68	2.97	-96	-122
-0.90	2.66	2.96	-95	-122
-0.80	2.64	2.94	-94	-121
-0.70	2.61	2.92	-93	-120
-0.60	2.59	2.90	-92	-119
-0.50	2.56	2.88	-91	-118
-0.40	2.53	2.86	-90	-117
-0.30	2.50	2.83	-88	-116
-0.20	2.47	2.80	-87	-114
-0.10	2.43	2.77	-86	-113
0.00	2.39	2.74	-84	-111
$+0.10$	2.34	2.70	-82	-110
$+0.20$	2.29	2.66	-80	-108
$+0.30$	2.24	2.62	-78	-106
$+0.40$	2.19	2.57	-76	-104
$+0.50$	2.13	2.52	-74	-101
$+0.60$	2.06	2.46	-71	-99
$+0.70$	1.99	2.40	-69	-96
$+0.80$	1.92	2.34	-66	-93
$+0.90$	1.84	2.27	-63	-90
$+1.00$	1.75	2.19	-60	-87
$+1.10$	1.66	2.11	-57	-83
$+1.20$	1.57	2.03	-54	-80
$+1.30$	1.48	1.94	-51	-76
$+1.40$	1.38	1.84	-48	-72
$+1.50$	1.28	1.75	-45	-69
$+1.60$	1.18	1.65	-42	-65
$+1.70$	1.09	1.55	-40	-61
$+1.80$	1.00	1.45	-38	-58
$+1.90$	0.91	1.35	-36	-54
$+2.00$	0.84	1.26	-34	-51
$+2.10$	0.77	1.17	-33	-49
Unmodified	2.96	3.21	-107	-133
Hsue[a]	2.604	2.918	-106.9	-137.4
ATM[a]		3.869		-138.1
Expt.[b]	0.90 ± 0.18		-52 ± 10	

[a]Reference 5.
[b]Reference 1.

TABLE V. The second virial coefficient β_2 and the average lateral interaction energy ϵ_2 of an isolated argon pair for various reference planes under the LJ model, with the lattice constant of the xenon monolayer as 4.26 Å, 4.28 Å, and 4.32 Å, respectively. Column 1 shows the location of the reference plane above the xenon layer.

Distance (Å)	β_2			ϵ_2 (K)		
	4.26 Å	4.28 Å	4.32 Å	4.26 Å	4.28 Å	4.32 Å
0.10	3.80	3.81	3.82	−676	−675	−672
0.20	3.73	3.74	3.75	−664	−663	−660
0.30	3.66	3.66	3.68	−651	−650	−647
0.40	3.58	3.58	3.60	−637	−636	−633
0.50	3.49	3.50	3.51	−622	−621	−618
0.60	3.40	3.41	3.42	−606	−605	−602
0.70	3.30	3.31	3.32	−590	−589	−585
0.80	3.20	3.21	3.22	−572	−571	−568
0.90	3.09	3.10	3.11	−554	−553	−549
1.00	2.98	2.98	3.00	−534	−533	−530
1.10	2.86	2.86	2.88	−514	−513	−510
1.20	2.73	2.74	2.75	−494	−493	−490
1.30	2.60	2.60	2.62	−473	−472	−469
1.40	2.46	2.47	2.48	−451	−450	−448
1.50	2.32	2.33	2.34	−429	−429	−426
1.60	2.18	2.18	2.20	−408	−407	−405
1.70	2.03	2.04	2.05	−386	−386	−384
1.80	1.89	1.90	1.91	−365	−365	−363
1.90	1.74	1.75	1.77	−345	−345	−343
2.00	1.60	1.61	1.63	−327	−326	−325

TABLE VI. The second virial coefficient β_2 and the average lateral interaction energy ϵ_2 of an isolated argon pair for various reference planes under the LJ model, with dielectric constant ϵ_d of the substrate as 5, 10, and 15, respectively. Column 1 shows the location of the reference plane above the xenon layer.

Distance (Å)	β_2			ϵ_2 (K)		
	5	10	15	5	10	15
0.10	4.08	3.95	3.90	−720	−697	−690
0.20	4.02	3.88	3.84	−710	−686	−678
0.30	3.96	3.82	3.77	−698	−673	−665
0.40	3.89	3.74	3.69	−686	−660	−652
0.50	3.82	3.66	3.61	−673	−646	−637
0.60	3.74	3.57	3.52	−659	−631	−621
0.70	3.65	3.48	3.42	−644	−614	−605
0.80	3.56	3.38	3.32	−627	−597	−587
0.90	3.46	3.27	3.21	−609	−578	−569
1.00	3.35	3.16	3.10	−591	−559	−549
1.10	3.23	3.04	2.98	−571	−538	−529
1.20	3.11	2.91	2.85	−549	−517	−507
1.30	2.97	2.77	2.71	−527	−494	−485
1.40	2.83	2.63	2.57	−503	−471	−462
1.50	2.68	2.47	2.42	−479	−447	−439
1.60	2.52	2.32	2.26	−453	−423	−415
1.70	2.36	2.16	2.11	−427	−398	−391
1.80	2.18	1.99	1.95	−400	−373	−369
1.90	2.01	1.82	1.78	−374	−349	−345
2.00	1.82	1.65	1.62	−347	−325	−322

The previous results[5] of including the Ne-Ne-Xe three-body effect are also shown in Table IV, with the same label for the argon case. The disappointing values indicate that the consideration of such effects will not improve the second-order properties significantly. However, the calculations in this work seem to imply that the Mahanty's image theory serves as another viable approach for the present system.

Before closing this section, three aspects should be mentioned here. First of all, one may worry about the deviations of both β_2 and ϵ_2 caused by the error of the lattice constant of the xenon monolayer. In Table V, we demonstrate the values of these two quantities calculated with lattice constants of 4.26 Å, 4.28 Å, and 4.32 Å, respectively. It is shown that these deviations with a variation of ± 0.02 Å of the lattice constant are less than 1%, which is much smaller than the experimental tolerance. Therefore, approximating the relatively complicated structure of the xenon monolayer by an average lattice constant of 4.30 Å introduces no substantial errors to the value of β_2 or ϵ_2. Second, we are surprised with the present calculations with the simplifying assumption that the substrate is treated as a perfect conductor. In reality, the image effect from the real substrate might not be so significant as from the perfect conductor. To probe the dependence on the dielectric constant of the substrate, we list in Table VI the calculations of β_2 and ϵ_2 based on three different values of dielectric constants. This table shows that the error in either β_2 or ϵ_2 is less than 1% with the dielectric constant $\epsilon_d \geqslant 15.0$. However, an error of 10% will arise when ϵ_d is taken as 5.0. One possible explanation and remedy for this error is inspired from the Mahanty's work.[17] According to his work, which was based on the jellium model, there is additional screening when the adatoms are actually embedded inside the metallic electrons that spill out of the surface. His results make the conclusion that the strength of the attractive interaction between two adatoms is only 12%, rather than 2/3, of the free-space value if one or two of these adatoms is or are inside the surface with surface-plasmon frequency equal to the principal adsorbate absorption frequency. Hence, this phenomenon offers possible compensation or accommodation of the less reduction of interatomic potential by the realistic substrate. Further work will be needed to completely clarify these issues. Finally, the uncertainty of the experiment is somewhat larger. Highly precise experiments may be needed for a more definite conclusion to arrive.

V. CONCLUSION

The second virial coefficient and its temperature derivative are recalculated for the physisorption of both argon and neon adatoms on xenon-plated graphite with the implementation of the image theory. In earlier works, the inclusion of three-body ATM contributions has not achieved satisfactory results for these cases. In order to fit the experimental measurements, the strength of the pairwise interaction must be lowered, without complete justifications, by an appreciable

amount from its gas phase value. In this paper, we obtain acceptable results when the reference plane, referred to as the ''ideal surface'' of the solid bulk, is set at 1.9 Å above the xenon plane. The self-consistency of the present work seems to indicate that the Mahanty's image theory can provide another approach in the consideration of the adsorption induced interactions.

ACKNOWLEDGMENTS

This work was supported by the National Science Council, Taiwan (Grant No. NSC88-2112-M007-048). One of the authors, C.-Y.R. is much indebted to Professor T. C. Choy for many useful discussions, especially about the Mahanty theory.

[1] M.W. Barnes and W.A. Steele, in *Fundamentals of Gas-Surface Interaction* (Academic, New York, 1967), p. 243.
[2] S.J. Ono, J. Chem. Phys. **18**, 397 (1950).
[3] S.T. Wu, Surf. Sci. **41**, 475 (1974).
[4] D.G. Brown and C.S. Hsue, J. Chem. Phys. **65**, 2501 (1976).
[5] C.S. Hsue and F.J. Lee, Surf. Sci. **69**, 472 (1977).
[6] W. Hogervorst and J. Freudenthal, Physica **37**, 97 (1967).
[7] J.M. Parson, P.E. Siska, and Y.T. Lee, J. Chem. Phys. **56**, 1511 (1972).
[8] C.Y. Ng and Y.T. Lee, J. Chem. Phys. **61**, 1996 (1974).
[9] B.M. Axilrod and E. Teller, J. Chem. Phys. **11**, 299 (1943); Y. Muto, Proc. Phys. Math. Soc. Jpn. **17**, 629 (1943).
[10] O. Sinanoğlu and K.S. Pitzer, J. Chem. Phys. **32**, 1279 (1960).
[11] A.D. McLachlan, Mol. Phys. **7**, 381 (1964).
[12] R.C. Brown, P.J. Dobson, and N.H. March, Phys. Lett. **54A**, 207 (1975).
[13] J. Mahanty and N.H. March, J. Phys. C **9**, 2905 (1976).
[14] B.C der Hertog and T.C. Choy, J. Phys.: Condens. Matter **7**, 19 (1995).
[15] L.W. Bruch, Surf. Sci. **125**, 194 (1983).
[16] S. Rauber, J.R. Klein, and M.W. Cole, Phys. Rev. B **27**, 1314 (1983).
[17] J. Mahanty, Phys. Rev. B **35**, 4113 (1987).
[18] K.D. Gibson, S.J. Sibener, B.M. Hall, D.L. Mills, and J.E. Black, J. Chem. Phys. **83**, 4256 (1985).
[19] K.D. Gibson, C. Cerjan, J.C. Light, and S.J. Sibener, J. Chem. Phys. **88**, 7911 (1988).
[20] R.A. Aziz, U. Buck, H. Jónsson, J.C. Ruiz-Suárez, B. Schmidt, G. Scoles, M.J. Slaman, and J. Xu, J. Chem. Phys. **91**, 6477 (1989).
[21] H. Margenau and N.R. Kestner, *Theory of Intermolecular Forces* (Pergamon, Oxford, 1971), Chap. 9.
[22] R.A. Aziz, in *Inert Gases*, edited by M. L. Klein, Springer Series in Chemical Physics Vol. 34 (Springer, New York, 1984), Chap. 2.
[23] A.D. Crowell and R.B. Steele, J. Chem. Phys. **34**, 1347 (1961).
[24] W. Hogervorst, Physica **51**, 59 (1971).
[25] R.J. Birgeneau and P.M. Horn, Science **232**, 329 (1986).
[26] Hawoong Hong, C.J. Peters, A. Mak, R.J. Birgeneau, P.M. Horn, and H. Suematsu, Phys. Rev. B **40**, 4797 (1989).
[27] M. Hamichi, A.Q.D. Faisal, J.A. Venables, and R. Kariotis, Phys. Rev. B **39**, 415 (1989), and references therein.
[28] M. Hamichi, R. Kariotis, and J.A. Venables, Phys. Rev. B **43**, 3208 (1991).
[29] Philip J. Davis and Ivan Polonsky, in *Handbook of Mathematical Functions With Formula, Graphs, and Mathematical Tables*, Nat. Bur. Stand. Appl. Math. Ser. No. 55, edited by M. Abramowitz and I. Stegun (U.S. GPO, Washington, D.C., 1966), p. 916.
[30] Philip J. Davis and Ivan Polonsky, in *Handbook of Mathematical Functions With Formula, Graphs, and Mathematical Tables*, (Ref. 29), p. 893.
[31] E. Zaremba and W. Kohn, Phys. Rev. B **13**, 2270 (1975).